




RESEARCH ARTICLE | APRIL 23 2019

The effect of adding an axial magnetic field on the expansion of a laser-produced plasma

G. Antar  ; A. Bahja; N. Metni  ; C. Habchi 



Phys. Plasmas 26, 043515 (2019)

<https://doi.org/10.1063/1.5089733>



View
Online



Export
Citation

29 April 2024 12:13:40

Physics of Plasmas

Features in Plasma Physics Webinars

Register Today!

The effect of adding an axial magnetic field on the expansion of a laser-produced plasma

Cite as: Phys. Plasmas **26**, 043515 (2019); doi: [10.1063/1.5089733](https://doi.org/10.1063/1.5089733)

Submitted: 22 January 2019 · Accepted: 1 April 2019 ·

Published Online: 23 April 2019







View Online



Export Citation



CrossMark

G. Antar,^{1,a)}  A. Bahja,²  N. Metni,³  and C. Habchi³ 

AFFILIATIONS

¹American University of Beirut, Riad El-Solh, Beirut 1107 2020, Lebanon

²Lebanese International University, Mousaitbeh, PO Box 146404, Mazraa, Lebanon

³Notre Dame University-Louaize, Zouk Mosbeh, PO Box 72, Zouk Mikael, Lebanon

^{a)}Electronic mail: gassan.antar@aub.edu.lb

ABSTRACT

We use a pulsed ultraviolet laser to ablate a copper target in order to study the effects of adding a permanent and axial magnetic field on the plasma plume expansion. The laser pulse duration is 20 ns, its energy is 150 mJ, and it is focused on a surface of about 1 mm². The target is inserted at the center of a ring permanent neodymium magnet as we compare data taken with and without the magnetic field using a Langmuir probe that is installed at 2.5 cm from the target but is capable of moving radially. The magnetic field, B , affects the plasma plume by reducing its expansion and by increasing the plasma temperature significantly. We report, and for the first time, the measurement of the average axial as well as the radial electric fields and show that both are enhanced in the presence of a magnetic field. This yields a strong increase in the plasma current and thus that of ohmic heating, which could help in explaining the temperature increase recorded by different groups when a magnetic field is added to the plasma plume expansion.

Published under license by AIP Publishing. <https://doi.org/10.1063/1.5089733>

I. INTRODUCTION

The intense interaction of lasers with solid targets is studied for many different applications like inertial fusion,¹ pulsed laser deposition (PLD) for thin film coating,² and laser induced breakdown spectroscopy (LIBS) used to detect and quantify the contaminants in samples.³ High energy laser beams are also proposed to propel objects in space providing the thrust needed for maneuvering and positioning objects in space.^{4–8} The ablative or the pulsed laser propulsion (ALP or PLP, respectively) is a direct method based on the principle of momentum transfer by the laser to the target.

Recent studies of the laser ablation suggested that adding a magnetic field (\vec{B}) to affect the plasma plume expansion for different reasons like enhancing thrust, increasing thin film thickness, removing debris, and ameliorating the spectroscopic measurements. We divide the usage of a permanent magnetic field to affect the dynamics, ionization, and optical as well as thermal properties of the plasma into two categories following the direction of \vec{B} , parallel or perpendicular to the main expansion direction of the plasma plume.

Most of the experiments reported in the literature were made in situations where a transverse magnetic field is used to affect the plasma plume. Begimkulov *et al.*⁹ reported the generation of a plasma jet with

enhanced light emission from multiple ionized species in the presence of a transverse magnetic field. The usage of spectroscopic measurements of carbon plasma was done by Harilal *et al.*¹⁰ to infer the plasma temperature and density. The effect of the nonuniform transverse magnetic field applied on the carbon plasma was investigated using fast imaging where it was noted that the plasma expansion has two time scales and temporal oscillations.^{11,12} Harilal *et al.* used fast imaging and spectroscopy to characterize the aluminum plasma as it expands across a transverse magnetic field.¹³ They reported a temperature increase in the plume due to Joule heating and adiabatic compression while a slow-down of the axial motion. No or little effect was found on the plasma density when the transverse magnetic field was applied but it had an effect on debris mitigation for coating purposes.¹⁴ This was confirmed later by Pagano *et al.*¹⁵ who reported an enhancement of the intensity of some neutral and ion emission lines. Langmuir probes were used to study the plasma plume expansion in a transverse magnetic field where the electron plasma temperature was found to increase with the laser energy and magnetic field.¹⁶ This was confirmed by Pandey and Thareja¹⁷ with spectroscopic measurements.

For cases with \vec{B} parallel to the plasma plume axis, Okada *et al.*¹⁸ were able to modify the properties of the plasma plume generated by the laser impacting a thin aluminum target. In the presence of a

uniform magnetic field, a nearly cylindrical plasma column was detected. In order to enhance the coating properties of the PLD and in continuation to the “Aurora”^{19,20} and “Eclipse-Aurora”²¹ PLD techniques, García *et al.*²² used a nonuniform magnetic field with the direction parallel but pointing in the opposite direction to the plume expansion. A similar experiment was done by Torrisi *et al.* who used a strong magnetic trap to modify the plasma plume expansion. They showed using optical diagnostics an increase in the plasma ion energy due to the presence of the magnetic field trap.²³ Axial and pulsed magnetic fields were produced by a planar induction coil that was inserted 1 cm from the target producing a magnetic field of 0.3 T. The authors reported enhancement in the visible light emission accompanying compression and plasma heating.^{24,25} Plasma focusing caused by an axial magnetic field was also characterized using an intensified charge-coupled device (ICCD) camera as well as spectroscopic diagnostics.²⁶ They confirmed that the presence of the magnetic field leads to an increase in the electron temperature but a decrease in the plasma density. The axial magnetic field trap was also applied by Favre *et al.*, and the plasma properties were investigated using plasma imaging, spatially resolved optical emission spectroscopy, and Faraday cup.²⁷ Their observations concluded evidence of radial and axial plasma confinement due to the magnetic field gradients.

Most of the references presented evidence of an increase in the plasma temperature. In the work of Roy *et al.*,²⁶ they added: “Although a magnetic field cannot accelerate ions, it can perturb the electrical field developed inside the plasma that produces the acceleration of the ions ejected from the nonequilibrium plasma.” The measurement of the electric field is the main subject of this work, which thus comes to complement the previous contributions in order to help clarifying the behavior of the plasma plume in the presence of an external magnetic field.

In this paper, we compare the plasma properties using a Langmuir probe in the presence and absence of a permanent and axial magnetic field. Our setup uses an axial magnetic field generated by one ring magnet with a direction parallel to the plasma propagation motivated by the quest to increase the plasma pressure. In Sec. II, we discuss the various components of the experimental setup as well as the probe technique used to obtain the plasma properties. In Sec. III, we report a net increase in the plasma temperature in agreement with previous investigations. The main contribution of this paper presented in Sec. IV is the measurement of the axial and radial electric fields deduced, respectively, from the time dependence on the radial values of the space potential; a net increase in their values is detected in the presence of the axial magnetic field. The reduction of the plasma plume expansion is discussed in Sec. V where the ion saturation is recorded as a function of radial distances.

II. EXPERIMENTAL PROCEDURE

The aim of this experiment is to understand the effect of a non-uniform axial magnetic field on the plasma produced by a laser pulse. The target is inserted into a ring neodymium magnet and the plasma plume is characterized with a Langmuir probe. Below, we describe each of the components of the experimental setup.

A. The pulsed laser deposition setup

The laser is a KrF Excimer emitting at the wavelength of 248 nm, which is in the ultraviolet range of the electromagnetic spectrum. The pulse duration is 20 ns with a repetition rate that can be varied from 5 to 50 Hz and energy that can reach up to 750 mJ; for this study, the

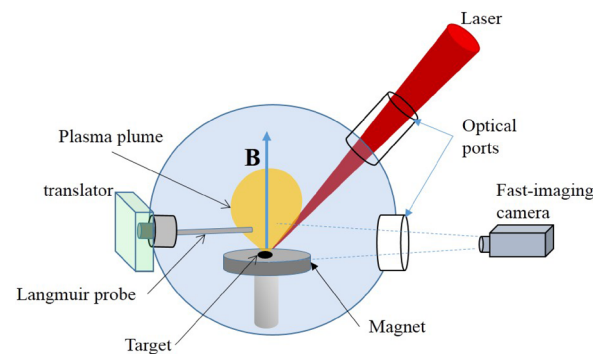


FIG. 1. Schematic of the experimental setup with the laser focused on the target, which is installed inside a permanent ring magnet. The Langmuir probe operates in a single mode and is positioned at $Z_0 = 2.5$ cm from the target while its radial position can be modified. A side window allows fast imaging of the plasma plume.

repetition rate is set to 20 Hz and the energy to 150 mJ. The beam is focused on the target by a lens to reach a surface of about 1×2 mm² causing the ablation. The experimental setup is illustrated in Fig. 1. It consists of a cylindrical stainless-steel vacuum chamber with dimensions approximately 0.5 m in height and diameter where the pressure can be as low as 10^{-7} mbar. In order to minimize the coating on the optical windows, we introduce Argon gas up to 10^{-5} bar. Considering 5 eV electrons, the mean free path for inelastic electron-neutral collision is about 5 cm that is greater than the distance between the plasma source and the probe. Consequently, we neglect the ionization of the argon atoms by the plasma. However, at the distance of laser optical window, that is about 30 cm, many collisions take place, hence minimizing its coating by the copper vapor.

B. The copper target

For this investigation, we use copper as a target mainly because it is not a magnetic material; consequently, it does not modify the ambient magnetic field of the permanent magnet. Moreover, it has relatively low boiling and melting temperatures as well as low ionization energy, which requires lesser laser energy to produce plasma. In Table I, we insert key thermo-physical properties of the copper target.

The copper target is cut to fit inside the ring magnet and cleaned before being submitted to the laser energy pulse. It is then installed at its center as shown in Figs. 3(a) and 3(b). Another target holder is used so that the laser has the same footprint on the target with and without the permanent magnet.

The plasma expansion is imaged with an exposure time of 10 μ s and the sample is shown in Fig. 2 in the absence of the magnetic field.

TABLE I. Main thermo-physical properties of the copper target.

Melting temperature [K]	1358
Boiling temperature [K]	3200
First ionization energy [kJ/mole]	745.5
Thermal conductivity [W/m K]	400
Reflectivity	0.35
Absorption coefficient [1/m]	8.83×10^7

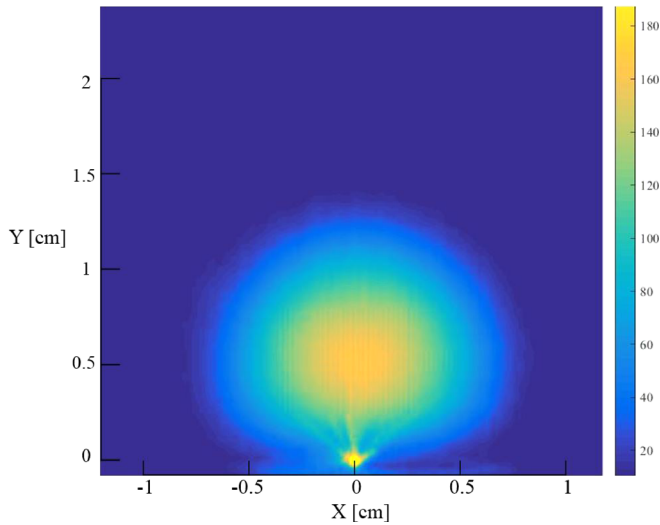


FIG. 2. A picture of the plasma plume in the absence of the magnetic field taken with an exposure time of $10 \mu\text{s}$. The color-bar to the right represents the light intensity in arbitrary units.

It illustrates rather well the free expansion from the point of impact of the laser on the target. The light intensity coming from the plasma is shown to occupy a semispherical region.

C. The static magnetic field

The static magnetic field is generated by a grade N42 neodymium ring magnet with a height of 1.25 cm and inner and outer radii, respectively, equal to 1.25 and 4.44 cm with axial magnetization. The axial magnetic field of the ring magnet, B_z , is measured as a function of the vertical axis Z at the magnet center $R = 0$ and plotted in Fig. 3(c). For $Z > 2.5 \text{ cm}$, the best fit shows the axial magnetic field decreasing according to Z^{-2} , whereas for $Z < 2.5 \text{ cm}$, this decrease is only linear according to Z^{-1} . Consequently, the position of the Langmuir probe at $Z = 2.5 \text{ cm}$ is at the edge of the region where the magnetic field diverges and where $B_z \simeq 150 \text{ G}$. The magnetic field expression for a ring magnet can be found in Refs. 28 and 29 where the analytical expression is obtained for the three components of \vec{B} .

D. The Langmuir probe

In this paper, we use the Langmuir probe to assess the plasma properties at a constant $Z_0 = 2.5 \text{ cm}$ from the target but with the capability to move in the radial direction. It enables us to get the plasma density (n_e), temperature (T_e), and space potential (V_{sp}) at different locations in the plasma plume. We assume that the plasma at the measurement distance is quasi-neutral and singly ionized. The former assumption is justified since no addition or subtraction of the plasma species, either electrons or ions, takes place. The latter is reasonable because although multiple ionization may take place at the laser-surface interface, the highly energetic population rapidly redistributes its energy to form a singly ionized plasma because of the high collision frequency.

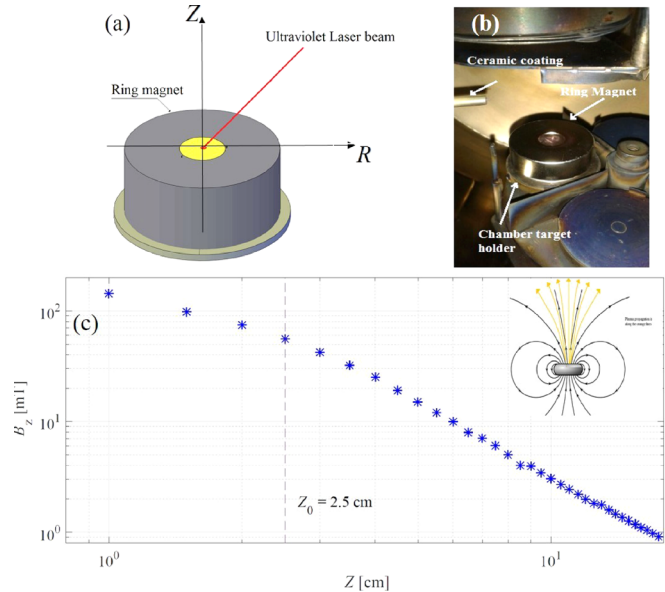


FIG. 3. In (a), we illustrate the way the target is simply inserted in the Neodymium ring magnet. (b) An actual image of the copper target-neodymium ring assembly. (c) The measured axial magnetic field B_z as a function of distance to the target Z . We also illustrate the magnetic field lines in a ring magnet showing that at 2.5 cm away from its surface, the magnetic field has an axial as well as a radial component.

E. The Langmuir probe setup

The Langmuir probe used to perform our measurement is composed of a $r_p = 0.5 \text{ mm}$ tungsten wire inserted into a Lanthanum hexaboride ceramic (LaB_6) tube for thermal insulation as well as electrical isolation. Only $h_p = 1 \text{ mm}$ emerges from the ceramic tube making the area of the probe to be $A_p \simeq 1.8 \text{ mm}^2$. The probe current collected from the plasma increases linearly with the area. Consequently, the dimensions of our probe are chosen, on one hand, to have enough current leading to a good signal-to-noise ratio and, on the other, to limit the probe perturbation of the plasma plume. The probe is biased by a Kepco power supply that is set at a constant potential (V_{bias}) and the current is measured as a potential drop across a 50Ω resistor. A Lecroy differential amplifier (DA1855) with a bandwidth of 100 MHz is used to bring the measurement around 0 V before the signal is digitized by a numerical Agilent oscilloscope (DSO5012A) at a frequency of 10 MHz. The current collected by the probe, for a given bias potential, is averaged over 20 laser pulses, a sufficient number to reduce the fluctuations associated with the reproducibility of the plasma as detected by the probe. Then, with the same experimental parameters, we change only the applied bias voltage between $V_{bias} = -4.5$ and $+4.5 \text{ V}$ after having verified that this range is sufficient to obtain the temperature, the density, and the space potential of the plasma. The same acquisition time and trigger are used for all the data; consequently, at each time step, we obtain an IV-trace as the current is plotted as a function of the bias potential. The cylindrical probe is positioned at a given radial distance to the magnet axis, denoted by R , as we record the data as a function of time.

F. The Langmuir probe theory

According to the Langmuir probe theory,³⁰ in the range where ions dominate, the current collected by the probe has the expression

$$I = A_s j_{sat} \left(1 - \exp \frac{e(V_{bias} - V_F)}{k_B T_e} \right). \quad (1)$$

The floating potential, denoted by V_F , is the voltage at which the ion current is exactly equal to the electron current leading to a zero total net current. For $V_{bias} \ll V_F$, the probe is in the ion saturation regime with a current density $j_{sat} = 0.6en_e c_s$, where $c_s = \sqrt{k_B T_e / M_i}$ is the ion sound speed assuming $T_i \ll T_e$. The ion mass is that of copper $M_i = 1.055 \times 10^{-25}$ kg, the elementary electric charge is e , and the Boltzmann constant is k_B . In the range of plasma densities investigated here, the sheath thickness remains quite small with respect to the probe area, hence leading to $A_s \simeq A_p$. On the other hand, when comparing magnetized to unmagnetized plasmas, one needs to take into account the magnetization of electrons and ions. In our case, considering the ambient magnetic field and the plasma temperatures, the electron Larmor radius is smaller than the probe size, whereas the ion Larmor radius is much greater. Consequently, the ion saturation current which depends on n_e and ion dynamics is not modified. Moreover, the exponential increase in the current around the floating potential also remains valid.³⁰ Further discussion on cylindrical probes in the presence of a magnetic field can be found in Ref. 31.

In Fig. 4(a), we plot the probe current, I , for $R=0$ and an applied voltage $V_{bias} = -3.2$ V as a function of time. Each curve is an average over 20 time traces obtained using 20 laser pulses. This reduces the error bars of the IV-traces as reflected in Fig. 4(b) where we plot I as a function

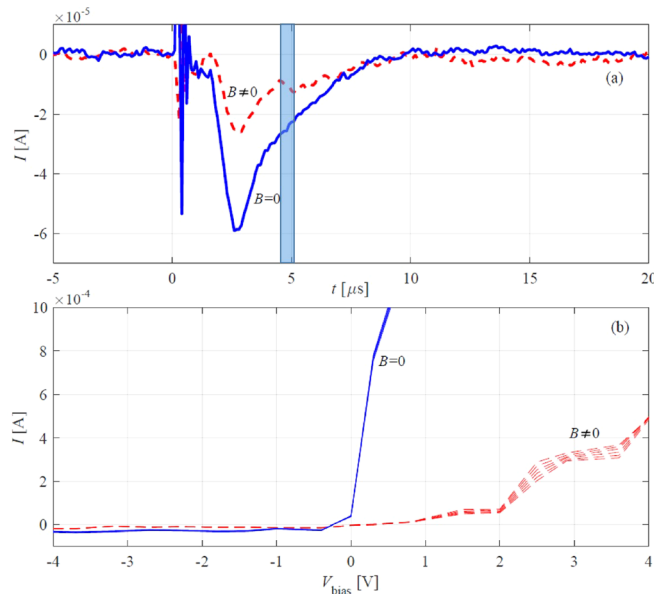


FIG. 4. (a) The probe current I as a function of time for the two cases with (dashed line) and without (solid line) the external magnetic field for a bias voltage, $V_{bias} = -3.2$ V and $R=0$. The colored rectangle at around $t \sim 5 \mu s$ indicates the region where the IV-traces are shown in (b). In (b), we show the IV-traces reflecting I as a function of the biased potential V_{bias} for $B=0$ in the solid line and $B \neq 0$ in the dashed line. For each magnetic field, 6 different IV-traces are plotted.

of V_{bias} . From (a), one can deduce that the current increases abruptly in time and then decreases with a longer time constant. The total duration of the plasma at the probe tip is estimated to be about $10 \mu s$. Note that the amount of current drawn by the probe from the plasma is around 0.1 mA, reaching a maximum of 1 mA when the probe is in the electron saturation region. The shaded rectangle in (a) illustrates the period of time during which the six IV-traces, with and without B , are plotted in Fig. 4(b). It is clear that with and without the external magnetic field, the behavior as a function of the applied voltage changes drastically. In the ion saturation region, a higher current is reported for $B \neq 0$ and then for $B=0$. We also record a much faster increase in the current with respect to V_{bias} , which is a consequence of a lower temperature since the slope around the floating potential is inversely proportional to the electron temperature. As expected from the theory, the addition of the external magnetic field strongly reduces the electron saturation current from 5 mA (not shown in the figure) to about 0.3 mA.

G. The measurement method

The plasma parameters are obtained by fitting the region around the floating potential by an exponential function giving the measurement of T_e . Then, using the value of the ion saturation current I_{sat} and T_e , we get the density n_e . From the value of the floating potential (V_F), which corresponds to $I=0$, and T_e , the space potential is obtained according to the equation

$$V_{sp} = V_F - T_e \log \left(0.6 \sqrt{\frac{2\pi m_e}{M_i}} \right), \quad (2)$$

where m_e is the electron mass. Since we have the space potential at different radial positions and in time, one can assess the electric field. A recent study by Martin *et al.*³² confirmed the agreement between the voltage-sweeping Langmuir and an emissive probe for the determination of the space plasma potential.

H. Error analysis

The signal-to-noise ratio in our measurements is large as one can deduce from the plots in Fig. 4(a), which shows the raw current signals from the probe. The noise, detected for $t < 0$, is on the order of $1 \mu A$ whereas the signal amplitude is on the order $60 \mu A$; consequently, the signal-to-noise ratio in our measurement is about 50.

Concerning the measurement errors, we wish to emphasize that each of the plots in Fig. 4(b) taken with $B=0$, and $B \neq 0$, contains 6 different IV-traces obtained at times around $5 \mu s$ shown in the shaded area in Fig. 4(a). It is hard to see the difference between them indicating a low level of noise and a high level of signals reproducibility. This causes the smooth dependence of the plasma properties on time as reported in Figs. 5–9. The low level of noise is partly caused by the average that we perform over (only) 20 laser pulses for each time trace, which reduces the noise level associated with the reproducibility of the plasma as it comes in contact with the probe. The recorded level of fluctuations of the ion saturation current density is estimated to be about 10%.

The floating potential depends on the space potential and the temperature. However, the error made by deducing V_F from the curves can be amplified by the slope of the curve around $I \simeq 0$. Accordingly, the error in determining the floating potential is linked to the change

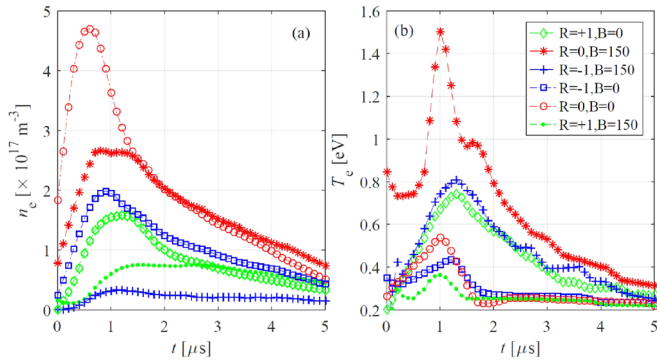


FIG. 5. (a) The plasma density as a function of time at three radial positions and in the presence and absence of the magnetic field. At $R=0$, data with $B=0$ and $B=150$ mT are plotted in “○” and “*,” respectively; at $R=-1$ cm, with and without the magnetic field are plotted “□” and “+,” and at $R=+1$ cm we use “◇” and “●” for $B=0$ and $B\neq 0$. The same symbols are used in (b) where the electron temperature is plotted as a function of time.

in the density, which dominates the error of the ion saturation current, since $\delta j_{sat}/j_{sat} = \delta n_e/n_e + (1/2)\delta T_e/T_e$ and the slope around V_F , which is the inverse of the electron temperature. The error around the floating potential is thus $\delta V_F = \tan(1/T_e)/\delta j_{sat}$, where δj_{sat} is deduced from the fluctuation around the data for large negative V_{bias} .

The error around the space potential is then calculated according to $\delta V_{sp}/V_{sp} = \delta V_F/V_F + \delta T_e/T_e$ where $\delta T_e/T_e \sim 0.1$ and that of the electric fields as $\delta E_z/E_z = \delta V_{sp}/V_{sp}$.

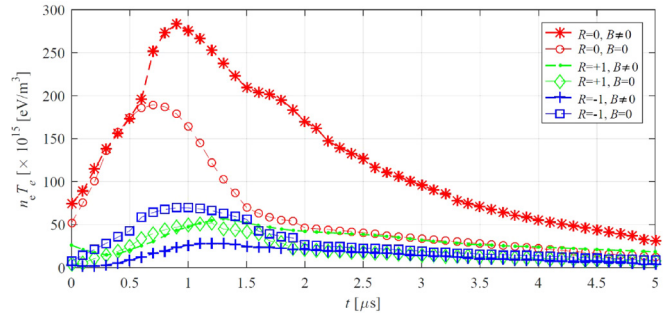


FIG. 6. The plasma pressure $n_e T_e$ as a function of time for the three radial positions with and without B .

III. DENSITY AND TEMPERATURE BEHAVIOR WITH AND WITHOUT THE MAGNETIC FIELD

In this section, we aim at discussing the behavior of the density and temperature as a function of time, for three different radial positions, $R=0$ and $R=\pm 1$ cm, in the presence or absence of the static magnetic field. The free expansion of the plasma leads to a decrease in the plasma density as a function of distance to the target. This issue was discussed by many authors experimentally using spectroscopic measurements¹⁰ and theoretically.^{33–35} This decrease has two main origins: (1) the free expansion into vacuum since what is generated in about 1 mm^2 occupies an area about $\pi(25)^2/2\text{ mm}^2$ that is about 1000 bigger.

Consequently, with free expansion alone, the density at $Z=2.5$ cm ought to be at least 1000 smaller than at $Z=0$. (2) During expansion,

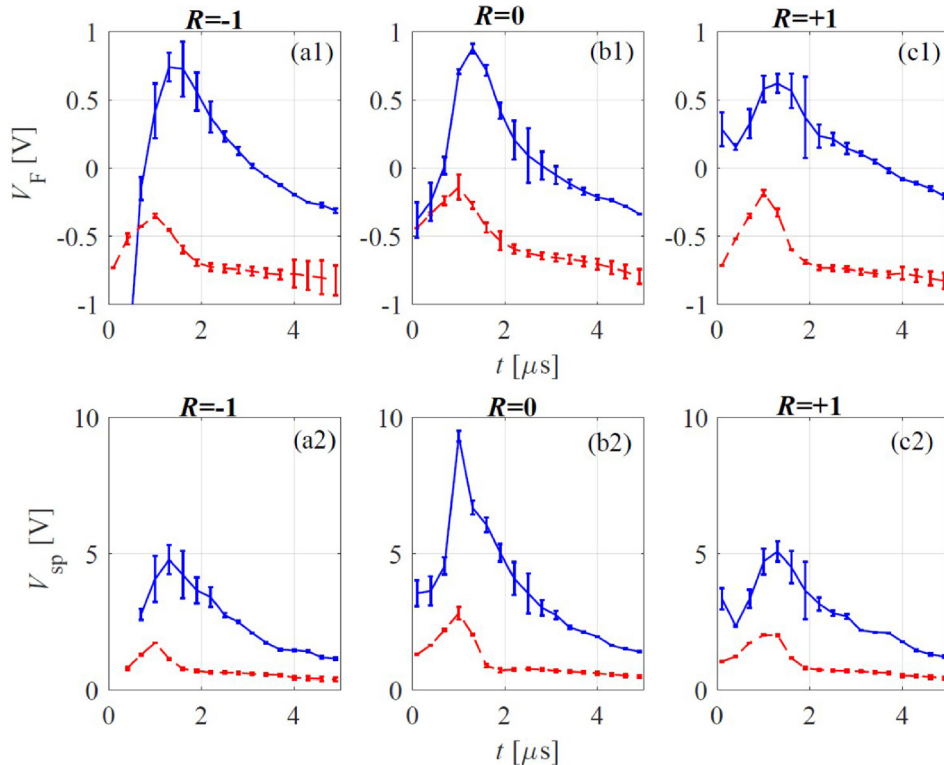


FIG. 7. (a1), (b1), and (c1) show the floating potential as a function of time, respectively, at three radial positions $R=-1, 0$, and $+1$ cm with (solid) and without (dashed) the external magnetic field. In (a2), (b2), and (c2), the same is plotted but for the space potential.

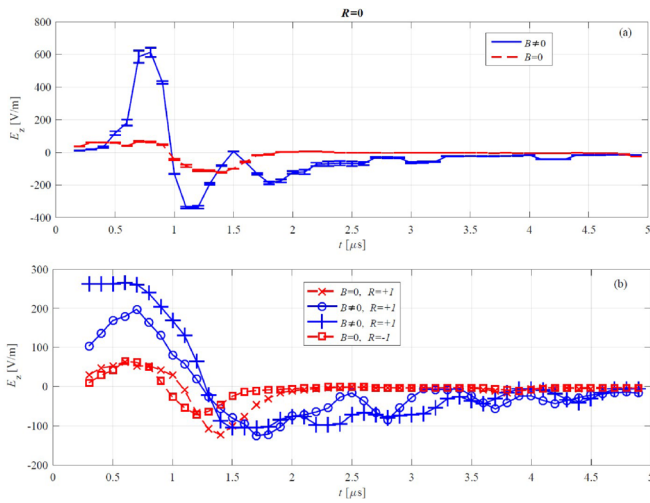


FIG. 8. In (a) and (b) the axial electric field E_z is plotted as a function of time at the three radial positions without and with the static magnetic field, respectively.

the plasma temperature drops favoring radiative as well as three-body recombination, which leads to a further decrease in the plasma density.

In Fig. 5(a), we show the average plasma density as a function of time and for the three radii at $R = 0, \pm 1$. The general trend is that n_e decreases when the static magnetic field is applied. For $R = 0$, the decrease is about 45%, whereas for $R = \pm 1$, it is even more pronounced reaching 75%. The radiative as well as the three-body recombination depends strongly on temperature; however, as it will be shown hereafter, the plasma electron temperature increases with the application of

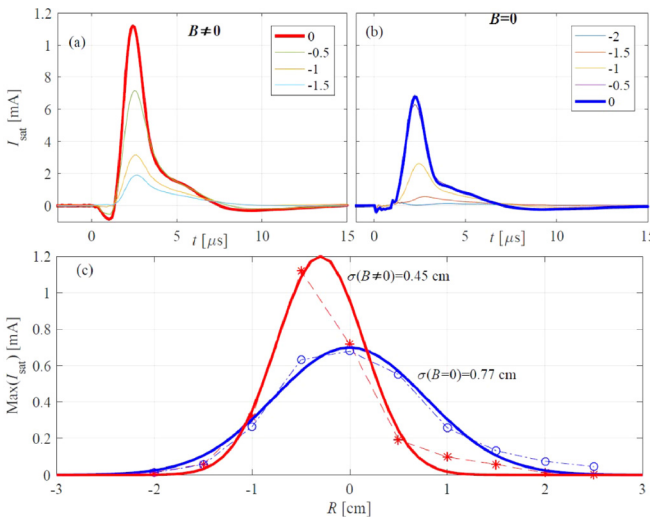


FIG. 9. In (a) and (b), we plot the ion saturation current I_{sat} as a function of time for four radial positions, respectively, for $B = 150$ mT and $B = 0$, the increment in the radial position being 0.5 cm. Note that $t = 0$ in these graphs is chosen before the increase in the density and is not the same as in previous figures. In (c), we show the maximum of I_{sat} as a function of the radial position R with (\star) and without (\circ) the magnetic field. We also inserted the best fit by a Gaussian profile and the width of the latter estimated by σ , the square root of the variance.

the magnetic field. Consequently, it is unlikely that the losses of the plasma density in the presence of B are due to recombination. The other cause is the changes in the plasma expansion. When applying the magnetic field, the plasma expansion ought to occur less strongly because of the confinement along the field lines. Consequently, one could interpret the decrease in the plasma density as caused by the confinement of the plasma plume leading to less density outside the axis defined by the laser-target interaction. A more detailed analysis of the ion saturation current where the dependence on R is performed with more accuracy presented hereafter supports this hypothesis.

In Fig. 5(b), we plot the electron temperature as a function of time at the three radial positions in the presence and absence of the magnetic field. The electron temperature increases rather strongly with the application of the magnetic field in agreement with previous spectroscopic measurements.^{12,36} At $R = 0$, T_e increases from 0.5 to 1.5 eV, that is by a factor of 3, for $R = \pm 1$, we record an increase from 0.4 to 0.8 eV, that is by a factor of 2.

Despite the decrease in density at the measured radial distances, the strong increase in the plasma temperature leads to an increase in the plasma pressure ($P_e = n_e T_e$) as depicted in Fig. 6. Consequently, by simply adding a permanent magnetic field around the target, one can enhance the momentum for thruster's application. The increase in the plasma plume temperature could also be used to change the coating properties of thin films when using the PLD.

We deduce that the plasma density and temperature are affected by the presence of a static magnetic field. At the locations investigated here, we note a decrease in the plasma density by about 50% but a net increase in the plasma temperature, which is multiplied by a factor of 3. In Sec. IV, we investigate the increase in the electric field because of adding a permanent magnetic field.

IV. BEHAVIOR OF SPACE POTENTIAL AND THE ELECTRIC FIELD

As indicated above, the point of zero current corresponds to the floating potential where the electron current equals the ion current. It is affected by the space potential of the plasma, which reflects the difference between the electron and the ion densities, and by the electron temperature. The behavior of the floating potential as a function of time is plotted in Fig. 7(a) for the three radial positions of the probe with and without B . The plasma potential changes not much for the three positions independently of the magnetic field; it increases and then decreases as the plasma plume passes by the probe tip. Without the magnetic field, V_F is mostly negative approaching 0 around 1 μ s. This behavior changes strongly with the application of B where V_F is now positive reaching 0.8 V and then decreases to become negative for $t > 3 \mu$ s. The floating potential behavior results from the space potential as well as the temperature; hence, it is hard to see the physics behind these changes and one needs to separate the two contributions.

We reconstruct the space potential of the expanding plasma V_{sp} from the measurements of V_F and T_e according to Eq. (2) and plot the results in Fig. 7(b). With and without the ambient magnetic field, the plasma is found to be positively charged, which is the consequence of the electrons being lighter, hence escaping faster than the ions the plasma plume. For $B = 0$, V_{sp} increases in time from 0 to about 2 V for the three investigated radial positions. For $B = 50$ mT, the space potential increases to 8 V for $R = 0$, that is by a factor of 4 with respect to

the free expansion case. For the other two radial positions, an increase by a factor of 2 is reported.

A. The axial electric field

In Fig. 7, we showed the time dependence of the space potential as the plasma plume passes by the probe. The plasma properties do change as a function of time during this passage. However, one can assume that we would have obtained the same result if the plume remained frozen in space and the probe moved in the opposite direction recording its properties in space. This equivalence between the spatial and temporal properties is called Taylor’s frozen flow hypothesis,^{37,38} according to which one can assume that the data obtained from the plume motion across the probe, that is in time, are the same as from a hypothetical probe motion across the plume, that is in space. This leads to the convective derivative which is equal to 0 and thus one may replace the time derivative by a space derivative according to

$$\frac{\partial}{\partial t} = -V \frac{\partial}{\partial z}.$$

The values of the convection velocity are determined as $V = Z_0/\tau_0$, where τ_0 is experimentally obtained from the time corresponding to the maximum of the density, and depicted in Table II.

The axial electric field is then calculated according to

$$E_z = -\partial_z V_{sp} = \frac{1}{V} \frac{\partial V_{sp}}{\partial t},$$

and the results are shown in Fig. 8 for the three radial positions in the absence and presence of the static magnetic field.

For $B = 0$ [Fig. 8(a)], the profiles are quite similar for the three probe positions with the electric field changing direction around $t = 1 \mu\text{s}$. For $t < 1 \mu\text{s}$, E_z is positive with a direction pointing away from the target. It thus acts on the ions to accelerate them and the electrons to decelerate them as expected since the electrons are more free to move because of their light weight when compared to the ions. The opposite happens for the $t \geq 1 \mu\text{s}$ where the sign of E_z is negative with an amplitude slightly greater for $R = 0$ than for $R \pm 1$ reaching 50 V/m. The fact that the amplitude is roughly the same for the three radii is reflective of the isotropic nature of the free expansion in the absence of the magnetic field.

With the application of the magnetic field, the temporal behavior of E_z and the change in its direction around 1–1.5 μs remain unchanged, that is, positive at first and then negative as it decays to 0. However, the amplitude of E_z strongly increases mainly in the axial direction where we report

TABLE II. The convection velocities (m/s) obtained from the time the plasma density reaches maximum according to $V = Z_0/\tau_0$.

	$B = 0$ [mT]	$B = 150$ [mT]
$R = -1$ cm	2.8×10^4	1.8×10^4
$R = 0$ cm	4.2×10^4	2.5×10^4
$R = +1$ cm	2.3×10^4	2.2×10^4

$$E_z(R = 0, B = 150)/E_z(R = 0, B = 0) \sim 10$$

$$E_z(R = \pm 1, B = 150)/E_z(R = \pm 1, B = 0) \simeq 4.$$

For $R = 0$ [Fig. 8(a)], the amplitude of the axial electric field reaches +600 V/m for its first maximum and then –300 V/m for the first minimum. For $R = \pm 1$ [Fig. 8(b)], we report $E_z \simeq +200$ V/m for the first maximum and –100 V/m for the first minimum.

When the properties of the plasma plume are compared with and without B , we note that the magnitude of the electric field changes drastically with the onset of a strong anisotropy reflected in the radial dependence of the electric field at the three investigated positions

$$E_z(R = 0, B = 0)/E_z(R \pm 1, B = 0) \simeq 1$$

$$E_z(R = 0, B = 150)/E_z(R \pm 1, B = 150) \simeq 3.$$

This behavior is consistent with the anisotropic nature of the imposed magnetic field.

B. The radial electric field

From the radial dependence of the plasma space potential, one can estimate the average radial electric field by calculating $E_r = -\Delta V_{sp}/R$. However, because the distance between two positions is rather large, that is 1 cm, the values obtained are a lower estimate of E_r . In the presence of B , the radial electric field is about –400 V/m, whereas without B , this value drops to –70 V/m. Accordingly, we also witness in the radial direction a strong increase in the electric field by a factor of 6. The radial electric field direction points inward toward the center of the plasma plume.

Let us assess the motion that results from these radial and axial electric fields and compare it to the free expansion assuming that the plasma expands at about the sound speed, which is on the order of 10^4 m/s for $T_e \sim 1$ eV. The radial electric field, coupled to the axial magnetic field of $B_z = 150$ mT at the location we are measuring, gives rise to a $\vec{E} \times \vec{B}$ motion and thus an azimuthal rotation of $V_\theta \sim 400/0.15 = 2.7 \times 10^3$ m/s that is about 3 times smaller than the sound speed. On the other hand, azimuthal rotation in the same direction is also generated by the axial electric field E_z coupled to the radial component of the static magnetic field B_r . For the permanent magnet that we are using, at 1 cm from the axis, the magnetic field is not only axial but also radial with an amplitude of about $B_r \simeq 10$ mT. The resultant azimuthal velocity is thus estimated to be $V_\theta = E_z/B_r = 600/0.05 \sim 10^4$ m/s, which is on the same order of magnitude as the axial velocity of the plasma plume. We thus highlight the fact that the velocities caused by the $\vec{E} \times \vec{B}$ drift alone, as a result of adding the external magnetic field, become important and are on the same order as the sound velocity.

We deduce that the addition of a static magnetic field leads to an important increase in the electric fields in the plasma plume. This naturally generates fluid motion, currents, and thus ohmic heating, which contributes to the increase in the plasma temperature.

V. EFFECT OF THE MAGNETIC FIELD ON THE PLASMA EXPANSION

In this section, we aim at confirming the confinement of the plasma caused by the static magnetic field. We investigate the behavior of the plasma plume as a function of the radial position with a resolution decreased to 0.5 cm using the ion saturation current obtained by

biasing the probe to a negative potential -5 V. The ion saturation current, collected at different radial positions, is plotted in Fig. 9 with [in (b)] and without [in (a)] the static magnetic field. The laser triggers the data collection at $t = 0$ and the signals reflect the plasma plume as it passes by the probe tip. A time average over 20 pulses is performed for each of the time traces.

The time dependence of I_{sat} indicates the existence of two behaviors, in agreement with previous results³⁹ and with the measurements of the density and temperature shown above, which persist with and without B . The current increases and decreases in about $3 \mu\text{s}$ reflecting most probably the front of the plasma plume, followed by a tail that extends the decay from 3 up to $6 \mu\text{s}$.

The maximum of the ion saturation current, obtained for each time trace, is plotted as a function of the radial position of the probe in Fig. 9(c). For $B = 0$, where the plasma is freely expanding, the profile is symmetric with a total width at $1/e$ about 0.77 cm deduced from the best fit of the experimental data with a Gaussian profile of the form $\exp(-R^2/2\sigma^2)$; the latter is also illustrated in the subplot. When the static magnetic field is applied, the best fit of the data gives $\sigma = 0.45$, hence reducing the expansion by about 40% at the axial position $Z_0 = 2.5$ cm. On the other hand, we note an increase in the maximum value of I_{sat} from 0.65 to 1.2 mA at $R = -0.5$ cm when the magnetic field is added.

With this study, we deduce that adding a static magnetic field leads to a focusing of the plasma plume in agreement with previous results.

VI. CONCLUSION

In this paper, we subject a copper target at the center of a permanent ring magnet to an UV laser; the laser pulses last 20 ns with an energy of 150 mJ. One advantage is the simplicity of the setup in applying a magnetic field to a freely expanding plasma. In order to obtain the plasma properties, we use a Langmuir probe inserted at $Z_0 = 2.5$ cm from the target but it is free to move in the radial direction. We obtain the IV-trace by fixing all the parameters except the bias voltage and record the data as a function of time. Then, at a given time, the probe current is plotted as a function of the applied voltage, and from these IV-traces, the plasma temperature, density, and space potential are obtained as a function of time and radial position.

Adding the permanent magnetic does not seem to change the plasma density in a drastic manner but does increase the plasma temperature significantly as well as the electric field while reducing the radial expansion of the plasma plume. The strong increase in the electric field could help explain the increase in temperature reported here and by other authors as a result of adding an external magnetic field.

REFERENCES

- S. Pfalzner, *An Introduction to Inertial Confinement Fusion* (CRC Press, 2006).
- D. B. Chrisey and G. K. Hubler, *Pulsed Laser Deposition of Thin Films* (John Wiley & Sons, New York, 1994).
- A. W. Miziolek, V. Palleschi, and I. Schechter, *Laser Induced Breakdown Spectroscopy* (Cambridge University Press, 2006).
- H. Yu, H. Li, Y. Wang, L. Cui, S. Liu, and J. Yang, "Brief review on pulse laser propulsion," *Opt. Laser Technol.* **100**, 57–74 (2018).
- L. Felicetti and F. Santoni, "Nanosatellite swarm missions in low earth orbit using laser propulsion," *Aerosp. Sci. Technol.* **27**(1), 179–187 (2013).
- C. R. Phipps, J. R. Luke, G. G. McDuff, and T. Lippert, "Laser-ablation-powered mini-thruster," in *High-Power Laser Ablation IV* (International Society for Optics and Photonics, 2002), Vol. 4760, pp. 833–843.
- W. O. Schall, H.-A. Eckel, and W. L. Bohn, "Laser propulsion thrusters for space transportation," in *Laser Ablation and Its Applications* (Springer, 2007), pp. 435–454.
- A. Rubin, S. Zaidi, and R. Miles, "Thrust vectoring of a laser-ablated plasma using permanent magnets and various materials," in *51st AIAA Aerospace Sciences Meeting Including the New Horizons Forum and Aerospace Exposition* (2013), p. 1079.
- U. S. Begimkulov, B. A. Bryunetkin, V. M. Dyakin, G. A. Koldashov, S. N. Priyatkin, A. Y. Repin, E. L. Stupitsky, and A. Y. Faenov, "Laser-produced plasma expansion in a uniform magnetic field," *Laser Part. Beams* **10**(4), 723–735 (1992).
- S. S. Harilal, C. V. Bindhu, R. C. Issac, V. P. N. Nampoore, and C. P. G. Vallabhan, "Electron density and temperature measurements in a laser produced Carbon plasma," *J. Appl. Phys.* **82**(5), 2140–2146 (1997).
- A. Neogi and R. K. Thareja, "Laser-produced carbon plasma expanding in vacuum, low pressure ambient gas and nonuniform magnetic field," *Phys. Plasmas* **6**(1), 365–371 (1999).
- N. Behera, R. K. Singh, V. Chaudhari, and A. Kumar, "Two directional fast imaging of plasma plume in variable magnetic field: Structure and dynamics of the plume in diamagnetic and non-diamagnetic limits," *Phys. Plasmas* **24**(3), 033511 (2017).
- S. S. Harilal, M. S. Tillack, B. O'shay, C. V. Bindhu, and F. Najmabadi, "Confinement and dynamics of laser-produced plasma expanding across a transverse magnetic field," *Phys. Rev. E* **69**(2), 026413 (2004).
- S. S. Harilal, B. O'Shay, and M. S. Tillack, "Debris mitigation in a laser-produced tin plume using a magnetic field," *J. Appl. Phys.* **98**(3), 036102 (2005).
- C. Pagano, S. Hafeez, and J. G. Lunney, "Influence of transverse magnetic field on expansion and spectral emission of laser produced plasma," *J. Phys. D: Appl. Phys.* **42**(15), 155205 (2009).
- J. D. Haverkamp, M. A. Bourham, S. Du, and J. Narayan, "Plasma plume dynamics in magnetically assisted pulsed laser deposition," *J. Phys. D: Appl. Phys.* **42**(2), 025201 (2009).
- P. K. Pandey and R. K. Thareja, "Plume dynamics and cluster formation in laser-ablated copper plasma in a magnetic field," *J. Appl. Phys.* **109**(7), 074901 (2011).
- S. Okada, K. Sato, and T. Sekiguchi, "Behaviour of laser-produced plasma in a uniform magnetic field-plasma instabilities," *Jpn. J. Appl. Phys. Part 1* **20**(1), 157 (1981).
- T. Kobayashi, H. Akiyoshi, and M. Tachiki, "Development of prominent PLD (aurora method) suitable for high-quality and low-temperature film growth," *Appl. Surf. Sci.* **197–198**, 294–303 (2002).
- S. Yata, Y. Nakashima, and T. Kobayashi, "Improved crystallinity of ZnO thin films grown by the 'aurora PLD method'," *Thin Solid Films* **445**(2), 259–262 (2003).
- M. Tachiki and T. Kobayashi, "Manipulation of laser ablation plume by magnetic field application," *Jpn. J. Appl. Phys. Part 1* **38**(6R), 3642 (1999).
- T. García, E. De Posada, M. Villagrán, J. L. S. Li, P. Bartolo-Pérez, and J. L. Pena, "Effects of an external magnetic field in pulsed laser deposition," *Appl. Surf. Sci.* **255**(5), 2200–2204 (2008).
- L. Torrisi, D. Margarone, S. Gammino, and L. Ando, "Ion energy increase in laser-generated plasma expanding through axial magnetic field trap," *Laser Part. Beams* **25**(3), 453–464 (2007).
- J. R. Creel and J. G. Lunney, "Compression and heating of a laser-produced plasma using single and double induction coils," *Appl. Phys. A* **124**(2), 124 (2018).
- J. R. Creel, T. Donnelly, and J. G. Lunney, "Heating and compression of a laser produced plasma in a pulsed magnetic field," *Appl. Phys. Lett.* **109**(7), 071104 (2016).
- A. Roy, S. S. Harilal, S. M. Hassan, A. Endo, T. Mocek, and A. Hassanein, "Collimation of laser-produced plasmas using axial magnetic field," *Laser Part. Beams* **33**(2), 175–182 (2015).
- M. Favre, H. M. Ruiz, L. S. Caballero Bendixsen, S. Reyes, F. Veloso, E. Wyndham, and H. Bhuyan, "Effects of a static inhomogeneous magnetic field acting on a laser-produced carbon plasma plume," *AIP Adv.* **7**(8), 085002 (2017).
- R. Ravaut, G. Lemarquand, V. Lemarquand, and C. Depollier, "Analytical calculation of the magnetic field created by permanent-magnet rings," *IEEE Trans. Magn.* **44**(8), 1982–1989 (2008).

- ²⁹R. Ravaut, G. Lemarquand, and V. Lemarquand, "Magnetic field created by tile permanent magnets," *IEEE Trans. Magn.* **45**(7), 2920–2926 (2009).
- ³⁰I. H. Hutchinson, *Principles of Plasma Diagnostics*, 2nd ed. (Cambridge University Press, 2002).
- ³¹M. Usoltceva, E. Faudot, S. Devaux, S. Heurax, J. Ledig, G. V. Zadvitskiy, R. Ochoukov, K. Crombé, and J.-M. Noterdaeme, "Effective collecting area of a cylindrical Langmuir probe in magnetized plasma," *Phys. Plasmas* **25**(6), 063518 (2018).
- ³²M. J. Martin, J. Bonde, W. Gekelman, and P. Pribyl, "A resistively heated CeB₆ emissive probe," *Rev. Sci. Instrum.* **86**(5), 053507 (2015).
- ³³P. Mora and R. Pellat, "Self-similar expansion of a plasma into a vacuum," *Phys. Fluids* **22**(12), 2300–2304 (1979).
- ³⁴A. V. Gurevich and A. P. Meshcherkin, "Ion acceleration in an expanding plasma," *Zh. Eksp. Teor. Fiz.* **80**, 1810–1826 (1981).
- ³⁵U. Samir, K. H. Wright, and N. H. Stone, "The expansion of a plasma into a vacuum: Basic phenomena and processes and applications to space plasma physics," *Rev. Geophys.* **21**(7), 1631–1646, <https://doi.org/10.1029/RG021i007p01631> (1983).
- ³⁶K. S. Singh, A. Khare, and A. K. Sharma, "Effect of uniform magnetic field on laser-produced Cu plasma and the deposited particles on the target surface," *Laser Part. Beams* **35**(2), 352–361 (2017).
- ³⁷G. I. Taylor, "Production and dissipation of vorticity in a turbulent fluid," *Proc. R. Soc. London Ser. A* **164**(916), 15–23 (1938).
- ³⁸G. I. Taylor, "The spectrum of turbulence," *Proc. R. Soc. London Ser. A: Math. Phys. Sci.* **164**, 476–490 (1938).
- ³⁹J. Brcka, M. Alunovic, A. Voss, and E. W. Kreutz, "Investigation of plasma expansion in the PLD process by means of an electrical probe," *Plasma Sources Sci. Technol.* **3**(2), 128 (1994).